
Stochastic forecasts of seawater intrusion towards sustainable groundwater management: application to the Korba aquifer (Tunisia)

Jaouher Kerrou · Philippe Renard · Fabien Cornaton ·
Pierre Perrochet

Abstract A stochastic study of long-term forecasts of seawater intrusion with an application to the Korba aquifer (Tunisia) is presented. Firstly, a geostatistical model of the exploitation rates was constructed, based on a multi-linear regression model combining incomplete direct data and exhaustive secondary information. Then, a new method was designed and used to construct a geostatistical model of the hydraulic conductivity field by combining lithological information and data from hydraulic tests. Secondly, the effects of the uncertainties associated with the pumping rates and the hydraulic conductivity field on the 3D density-dependent transient model were analysed separately and then jointly. The forecasts of the impacts of two different management scenarios on seawater intrusion in the year 2048 were performed by means of Monte Carlo simulations, accounting for uncertainties in the input parameters as well as possible changes of the boundary conditions. Combining primary and secondary data allowed maps of pumping rates and the hydraulic conductivity field to be constructed, despite a lack of direct data. The results of the stochastic long-term forecasts showed that, most probably, the Korba aquifer will be subject to important losses in terms of regional groundwater resources.

Keywords Seawater intrusion · Uncertainty · Geostatistics · Climate change · Tunisia

Introduction

Numerical models are frequently used to assess seawater intrusion problems (Iribar et al. 1997; Bear et al. 1999; Paniconi et al. 2001; Arfib et al. 2002; Brunner and Kinzelbach 2008; Milnes 2011) and to design optimal groundwater resources management schemes (Cheng et al. 2000; Mantoglou et al. 2004; Abarca et al. 2006; Alcolea et al. 2009). With the increasing debate on climate change and its potential impacts on groundwater resources worldwide (Eckhardt and Ulbrich 2003; Holman 2006; Scibek and Allen 2006; Bates et al. 2008; Hendricks Franssen 2009), groundwater models are more and more used for investigating the response of coastal aquifers to potential sea-level rise, or changes in recharge (Sherif and Singh 1999; Essink 2001; Ranjan et al. 2006; Werner and Simmons 2009).

Nevertheless, the modelling of seawater intrusion in coastal aquifers remains a challenge (Diersch and Kolditz 2002). Solving density-dependent flow and mass transport equations requires numerical methods that are very sensitive to space and time discretization. The difficulties are usually ignored by simplifying the problem either by reducing the problem dimensions (Kerrou and Renard 2010), modelling steady-state conditions, assuming homogenous model parameters, or simplifying the physics of the problem like in sharp interface models (Reilly and Goodman 1985). These issues are even more critical when the heterogeneity of the aquifer has to be accounted for.

Previous studies have shown the impacts of heterogeneity on seawater intrusion model predictions. Dagan and Zeitoun (1998), Naji et al. (1998) and Al-Bitar and Ababou (2005) used two-dimensional (2D) hypothetical domains with a sharp interface assumption. Other studies (Held et al. 2005; Abarca 2006) used 2D vertical cross-section models of seawater intrusion inspired by the Henry problem (Henry 1964). In this study, the aim is, among other points, to model transient density-dependent dispersive transport in a real-world aquifer with three-dimensional (3D) heterogeneity. In such case, the lack of data to estimate model inputs and their distributions in space and time leads to uncertainty in model predictions. In practice, the resulting uncertainties justify the need for stochastic models to help decision makers (Renard 2007),

Received: 17 August 2011 / Accepted: 25 September 2012
Published online: 10 November 2012

© Springer-Verlag Berlin Heidelberg 2012

J. Kerrou (✉) · P. Renard · F. Cornaton · P. Perrochet
Centre of Hydrogeology and Geothermics (CHYN),
University of Neuchâtel,
Rue Emile Argand, 11, 2000 Neuchâtel, Switzerland
e-mail: jaouher.kerrou@unine.ch
Tel.: +41-32-7182587
Fax: +41-32-7182603

which is illustrated, for example, by the work of Hassan et al. (2001), Pohlmann et al. (2002) and Lecca et al. (2011).

While Monte Carlo techniques are accepted as the most general approach to quantify uncertainty, they are only seldom used in practice for real seawater intrusion problems. This is due first to the high computational time for solving 3D density-dependent problems at a sufficiently high resolution while covering a regional-scale system. In addition, in many practical situations, the data are very often limited and the construction of a stochastic model of heterogeneity is difficult because one cannot easily infer the required statistics. Important uncertainties are also related to boundary conditions and source/sink terms. For example, uncertainty in extraction rates is very frequent in irrigated plains where no control of the extraction is made by the authorities (Custodio 2002; Werner 2010). Combining all those uncertainties implies additional computational loads and makes the numerical problem so demanding that often it is not deemed feasible even if it is well accepted that such type of model should be used to help decision making. In this paper, some solutions to those problems are proposed.

This work is the continuation of two previous studies. In the first (Kerrou et al. 2010a), the hydrogeology of the coastal aquifer of Korba in Tunisia and a deterministic numerical model of the aquifer system were presented. In the second study (Kerrou et al. 2010b), a stochastic model of the extraction rates was developed. The present paper presents three new aspects. A new method to model the heterogeneity of the aquifer is presented; the interaction between uncertainties resulting from heterogeneity and/or exploitation rates is analysed; and the possible long-term evolution of the system is investigated by using high-performance computing.

The paper is organized in six sections. Firstly, the results of the two previous studies are summarized. A new method to model the heterogeneity of the aquifer, based on geological logs and hydraulic tests, is described. Then the uncertainties resulting from the heterogeneity of the hydraulic conductivity field and/or from the extraction rates are analysed. In the final section, the evolution of the Korba aquifer system until 2048 is investigated accounting for the various sources of uncertainty and two possible climate scenarios.

A deterministic model of the Korba aquifer

Hydrogeological context

The Korba aquifer is located in northern Tunisia (Fig. 1). It covers about 400 km² and is bounded by the Mediterranean Sea on the eastern side. As a major source of freshwater, the unconfined aquifer is intensively exploited, mainly for irrigation purposes. It has been progressively invaded by seawater intrusion due to the uncontrolled exploitation (Kerrou et al. 2010a) which started in the early 1960s and which was estimated to be around 50 hm³/y during the last few decades. From the early 1980s to 2004, more than 9,000 wells were pumping

(DGRE 2000). Aquifer recharge mainly occurs through infiltration of precipitation, which is highly variable in space and time. It was estimated to range between 8 % and 30 % of the 420 mm/y average annual rainfall, which represents a recharge of 29 hm³/y on average (Kerrou et al. 2010a). The inequality between inputs and extractions led to seawater encroachment in the Korba aquifer, contaminating groundwater as far as 2 km inland in 2004. That situation has motivated numerous studies (Tarhouni et al. 1996; Khlaifi 1998; Paniconi et al. 2001; Slama et al. 2008; Kouzana et al. 2009; Kerrou et al. 2010a, b; Ben Hamouda et al. 2011). The main aquifer formation is of Pliocene age and consists of yellow sand with alternating clay and sandstone layers (Ennabli 1980). The thickness of the Pliocene formation is about 80 m in the central part of the area, reaching 250 m offshore and decreasing towards the west (Figs. 1 and 2). This formation is overlain by Tyrrhenian Quaternary rocks, which form a 1.2-km-wide strip parallel to the coastline all along the study area (Figs. 1 and 2), and are mainly composed of arenitic limestone and conglomeratic units (Oueslati 1994). In the south of the study area, the late Miocene formation, called the Somâa sands, represents an aquifer formation of secondary importance. It is mainly composed of thick fine sand layers of continental origin including conglomeratic levels and clay lenses for a total thickness reaching 400 m. Figure 2 displays the conceptual model of the Korba aquifer which was used to establish a 3D numerical model of density-dependent flow and mass transport in a transient regime.

The numerical model

In Kerrou et al. (2010a), a high-resolution 3D numerical model of density-dependent flow and mass transport was described. Because this model constitutes the base that will then be used for the stochastic analysis, a summary of its characteristics is presented here. The *GroundWater* three-dimensional finite element code (Cornaton 2007) was used. This software solves a wide range of physical problems: variably saturated and variable-density groundwater flow, mass transport, heat transfer, and groundwater age and life time expectancy. The code was validated (Cornaton 2007) by comparison with a large number of analytical or pseudo-analytical solutions and a series of standard benchmarks—e.g. the Henry problem (Henry 1964) and the Elder problem (Elder 1958).

To account for both the high well density and the heterogeneity of hydraulic conductivity, the 3D geometry of the assumed confined aquifer was discretized into 1.616 million pentahedral prismatic finite elements (0.842 million nodes) with 36 layers (Fig. 3). The mesh displays local horizontal refinement (e.g. close to the sea) with elements having a size varying between 50 and 200 m horizontally and an average layer thickness of 3 m in the main aquifer (Pliocene).

Steady-state boundary conditions (BCs) consist of prescribed head on the seafloor and constant lateral inflow along the northern limit of the Pliocene formation. The

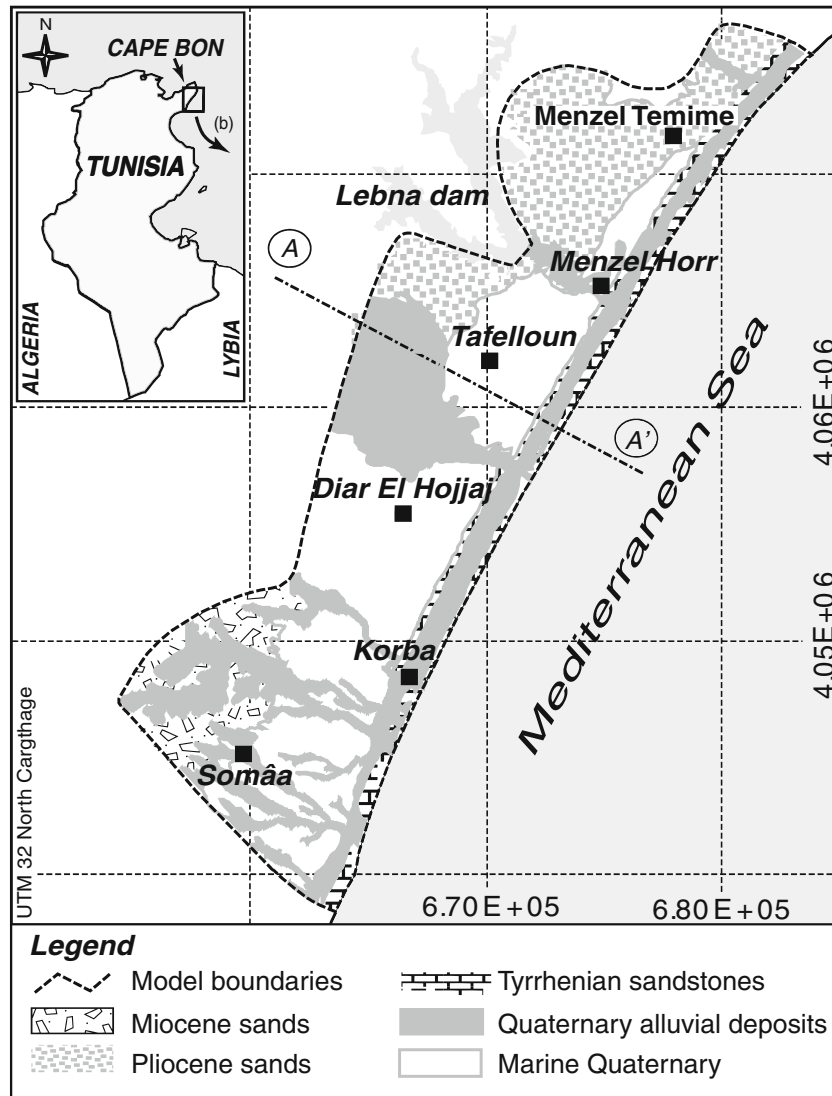


Fig. 1 Location map of Cape Bon, north-eastern Tunisia, and the Korba aquifer with the geological setting (AA' cross-section is shown in Fig. 2)

seaside boundary extends 3.5 km (arbitrarily fixed) offshore to allow an accurate estimation of hydraulic gradients seaside in addition to be a more realistic representation of the sea-boundary condition. The daily

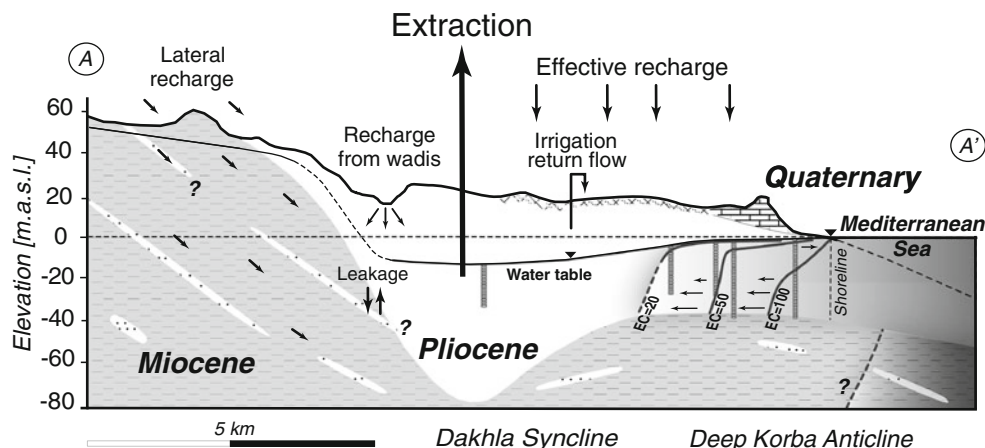


Fig. 2 Simplified geological cross-section (location in Fig. 1) of the Korba aquifer system illustrating the conceptual model based on up-to-date geologic and hydrodynamic data. The representations (interpolated by kriging) of aquifer surface and bedrock topography, and the August 2004 water table and seawater electrical conductivity (EC percent, grey lines), are also shown (Kerrou et al. 2010a)

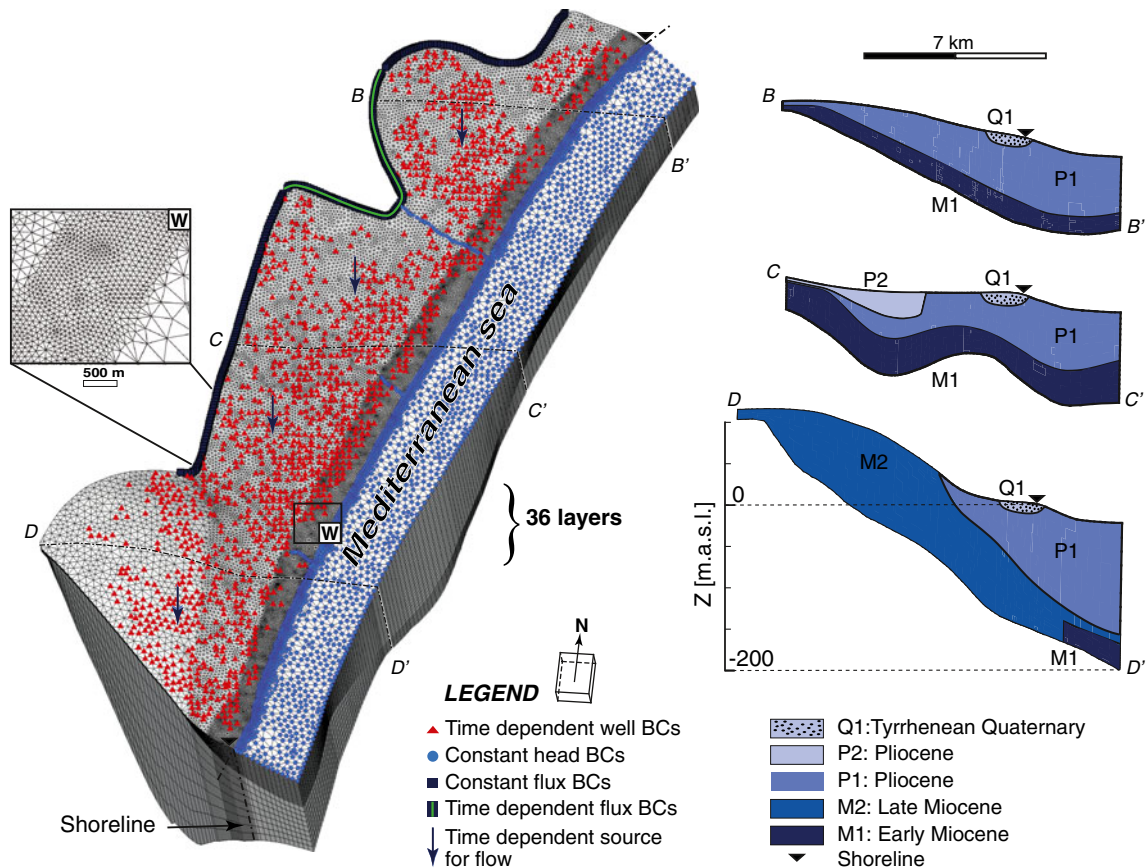


Fig. 3 The Korba aquifer 3D numerical model and three flow material cross-sections. Note that wells are attributed at the third slice and lateral fluxes are integrated on the thickness of the Pliocene formation only (modified from Kerrou et al. 2010a). BCs boundary conditions

Thornthwaite-Mather method (Steenhuis and Van der Molen 1986) was employed to estimate maps of the range of plausible recharge from 1960 to 2004 to constrain the interval of acceptable recharge during the calibration process. As an order of magnitude, the average recharge was estimated to $29 \text{ hm}^3/\text{y}$.

The transport boundary conditions are simple. A relative seawater concentration of 1 [–] is assigned on the seafloor to inward fluxes only (water enters the aquifer with seawater concentration but exits with the aquifer concentration). Note that the relative concentration is defined as the ratio between measured concentration everywhere in the domain and the concentration of dissolved salts in seawater. Freshwater recharging the aquifer has a relative concentration of zero.

Time-dependent conditions are prescribed during the transient simulation (1960–2004). The map of pumping wells locations is presented in Fig. 4. Time-varying discharge rates were defined based on estimations by the local authorities (Fig. 4e). The time-varying of the lateral influx and recharge were estimated from precipitation data. Note that for both transient simulations of flow and mass transport, steady-state solutions (without pumping) were used as initial conditions. During the transient simulation, the time-step is automatically adapted depending on the convergence of the solution with a maximum time-step of 90 days.

The calibration of the 3D model is described in detail in Kerrou et al. (2010a). In a first step, the mean hydraulic conductivity of the different geological formations and recharge rates were estimated in steady state. The storativity was estimated in a second step in a transient regime. The calibration of the flow was performed semi-automatically using PEST (Doherty 1998). The latter was constrained by freshwater head observations (1763 measures) and parameter ranges according to available information (e.g. pumping test data). After checking the stability of the numerical solution, the transport parameters were obtained by trial and error calibration in order to reproduce the observed saltwater encroachment (854 concentration measurements). The general aim of the whole calibration procedure was to fit the field observations and to reproduce the major regional features such as the depletion of the groundwater levels in the central part of the aquifer and the increasing salinity from 1960 to 2004. The resulting parameters are presented in Table 1. The root mean square error between observed and simulated heads was 6.2 m; for the saltwater concentrations, it was equal to 6.7 kg/m^3 . Those values and the corresponding scatter plots between simulated and observed values (Fig. 5) are considered acceptable for a 3D regional-flow model with homogenous parameters within each geological formation.

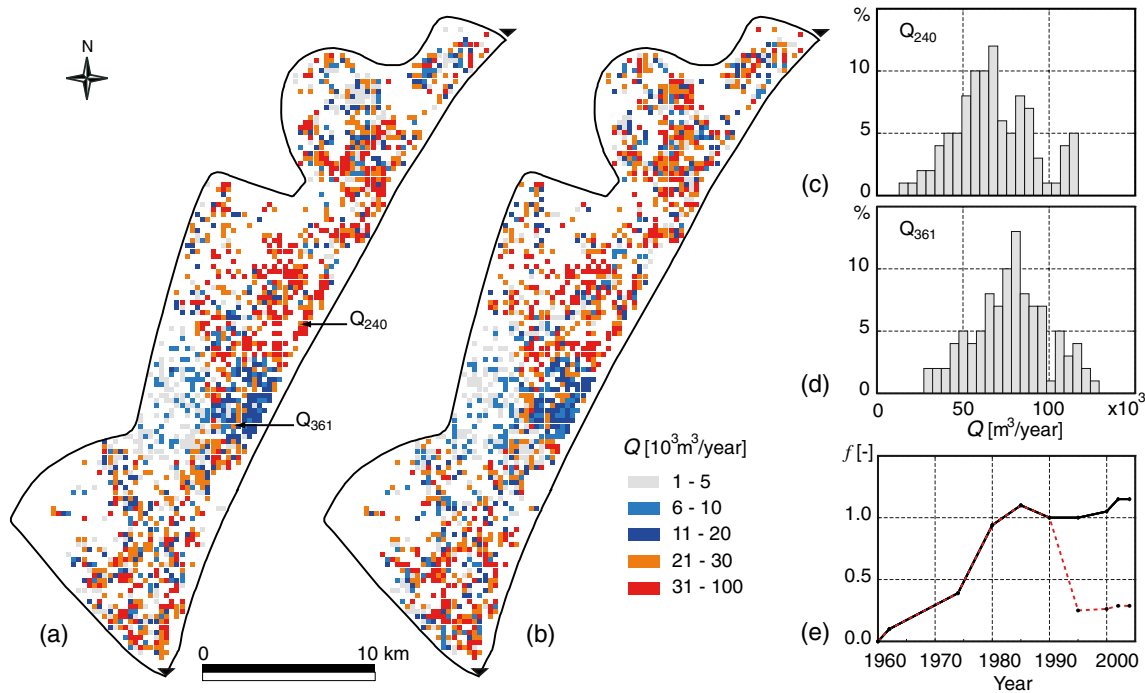


Fig. 4 a–b Two examples of the pumping rate maps (Q for 1996); c–d Histograms of pumping rates for two wells (240, 361); e Time-dependent evolution functions f [-] for both wells (solid black line for Q_{240} and gray dashed line for Q_{361}) with 1996 volume as reference (Kerrou et al. 2010b)

Modelling uncertain pumping rates

The Korba aquifer was exploited by more than 9,000 wells in the year 2000 for a total amount of groundwater abstraction of $50 \text{ hm}^3/\text{year}$. This situation of intensive exploitation is typical of most coastal aquifers around the Mediterranean Sea. Those coastal plains offer ideal conditions for food production and freshwater is then required for irrigation. The problem is that often there is no control of the extraction rates and only indirect data are available. In this situation, one needs to estimate the extraction rate from various sources of information. In a previous study (Kerrou et al. 2010b), a statistical model of the extraction rates was built.

The statistical model is based on a survey conducted in 1996 by the local authorities and the Institut National Agronomique de Tunisie; 432 wells in the central part of the domain were visited, their pumping rates were measured and their annual exploitation rates were estimated. This information was used to estimate the pumping rates over the whole aquifer by multi-linear regression. It was assumed that the pumping rate was correlated with some physical properties of the aquifer as well as some regional characteristics (e.g. high transmissivity allows high discharge; shallow depth facilitates groundwater abstraction; etc.). The parameters that were used are transmissivity, crop evapotranspiration, electrical conductivity, seasonal head variation, water-table depth, historical piezometric decline, distance to the sea, and topography. Those data were mapped on regular grids of $300 \times 300 \text{ m}$ resolution. The multi-linear regression allowed the estimation of the map of mean pumping rate over the whole aquifer. In addition, a

geostatistical analysis of the residuals between the estimated map and the measurements in the central area showed that the errors can be described by a Gaussian distribution of zero mean and a variogram having a sill of $2.1 \times 10^4 \text{ m}^3/\text{year}$ and a range of 700 m. This information was used to generate multiple equally-likely unconditional simulations of the residuals using the turning-band method (Matheron 1973; Tompson et al. 1989). Each of the 100 residual maps produced was then added to the average map (obtained by the regression) leading to 100 simulations of the extraction rates sharing all the same total extraction but distributed differently in space (Fig. 4). The temporal variation of the pumping rates is then modelled by rescaling the maps by two time-dependent functions (Fig. 4e). Additional details about this procedure are provided in Kerrou et al. (2010b).

Table 1 Model parameters

Parameter	Value
Seawater density [kg/m^3]	$1.025 \cdot 10^3$
Freshwater density [kg/m^3]	$1.000 \cdot 10^3$
Fluid viscosity [$\text{kg}/\text{m}\cdot\text{s}$]	$1.000 \cdot 10^{-3}$
Maximum relative concentration [-]	1
Average annual recharge [mm]	89
Hydraulic conductivity (isotropic) [m/s]: Q1; P1; P2; M1; M2	$2 \cdot 10^{-4}$; $1 \cdot 10^{-4}$; $5 \cdot 10^{-5}$; $6 \cdot 10^{-6}$; $1 \cdot 10^{-7}$
Storage compressibility [$1/\text{m}$]: Q1&P2;P1;M1;M2	$5 \cdot 10^{-3}$; $3 \cdot 10^{-3}$; $6 \cdot 10^{-4}$; $1 \cdot 10^{-4}$
Porosity [%]: Q1 & P1; P2 & M1 ;M2	10; 8; 5
Longitudinal dispersivity [m]	400
Transverse dispersivity [m]	40
Molecular diffusion [m^2/s]	10^{-8}

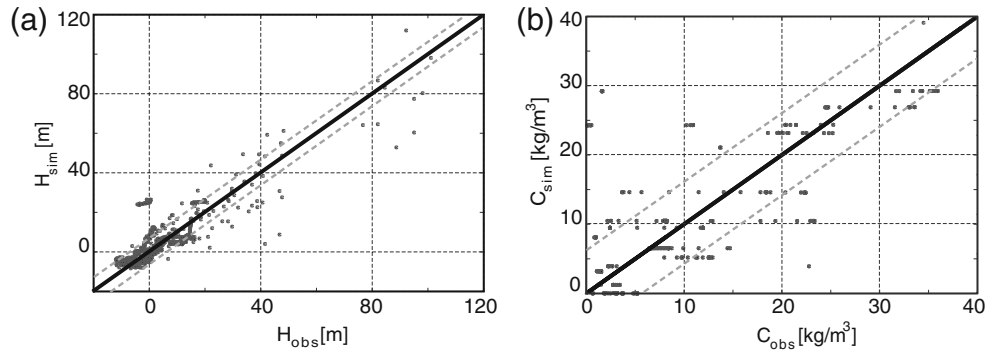


Fig. 5 Scatter plots showing the fits between the observed and simulated concentrations: **a** heads (H , m) and **b** salt concentrations (C , kg/m^3). In both cases, observed values \pm RMSE (root mean squared error) are also shown (*dashed lines*). Modified from Kerrou et al. 2010b

Modelling heterogeneity

As for the pumping rates, a specific method had to be designed to model the heterogeneity of the aquifer, despite insufficient data. This is one of the new methodological contributions of this paper. Because the technique is very simple and based on classical hydrogeological data, it is believed that it could be easily applied in other case studies.

The general idea of the proposed method is to use slug test and pumping test data (primary data) and detailed geological logs (secondary data) to generate realistic hydraulic conductivity profiles along the boreholes. The primary data allows to infer the first two moments of the probability distribution of the hydraulic conductivity. The secondary data allows to characterize the vertical variability of the hydraulic conductivity along the boreholes. When the hydraulic conductivity profiles are generated, one can use them together with the primary data to calculate the correlation scales, and further as conditioning data in a traditional multi-Gaussian framework to generate stochastic 3D hydraulic conductivity fields.

In the Korba aquifer, the characterization of the heterogeneity was focused on the Pliocene formation because it

represents the main aquifer. Two main datasets were used. The first consists of 15 hydraulic conductivity data estimated from slug tests completed in the Pliocene formation. In general, the slug test technique presents the advantage of being cheap and quick in practice. In the Korba aquifer, the slug tests were carried out by rapidly submerging a sufficiently heavy waterproof metallic cylinder into piezometers after installing pressure data loggers. The target was to create significant instantaneous rise and drawdown of the water table in the order of 1 m. Pressure data for both drawdown and recovery were then processed and interpreted mainly using Cooper et al. (1967) and Hvorslev (1951) models. While the pumping tests provide relatively large-scale averages of hydraulic conductivities, slug tests allow the characterisation of smaller scale heterogeneity. The hydraulic conductivity estimated from the slug tests varied between 1.3×10^{-4} m/s and 7×10^{-7} m/s with a variance $\sigma_{\ln k}^2 = 1.5$.

The second data set consists of 36 lithostratigraphical logs located mainly in the central part of the aquifer (Fig. 6a) and provided by the regional water management authority in Nabeul (Tunisia). Those data describe the vertical distribution of the lithotypes within the Pliocene formation.

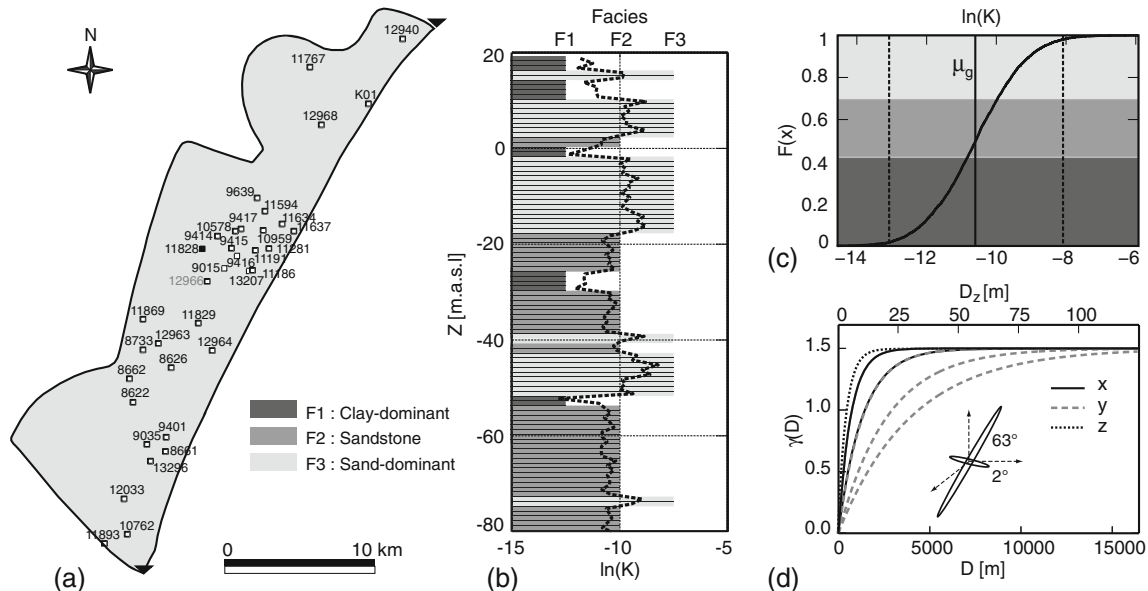


Fig. 6 Geostatistical model of hydraulic conductivities. **a** borehole location **b** one example of a lithostratigraphical log with random $\ln(K)$ values simulated with respect to the facies type **c** CDF of the Gaussian $\ln(K)$ distribution **d** directional variograms ($\gamma(D)$); note that six scenarios were considered (see Table 2)

A trial was made to use a truncated plurigaussian technique (e.g. Mariethoz et al. 2009) to model the geological heterogeneity, but the primary data set was not sufficient to calculate reliable variograms (Grava 2005). It was then decided to combine the available primary data in a simple and original manner to provide realistic 3D representation of the hydraulic conductivity field. First, the 36 geological logs were analysed and assigned to three main lithotypes: sand-dominant, sandstone and clay-dominant with a resolution of 1 m (Fig. 6a and b). The lithotype logs were then converted into hydraulic conductivity values. To do so, a Gaussian distribution of the logarithm of the hydraulic conductivities was assumed. Its variance was estimated from the slug test data, and its mean was computed according to the following consideration. Since the horizontal effective hydraulic conductivity significantly controls the seawater wedge penetration (Abarca et al. 2007; Kerrou and Renard 2010), the equation of Ababou (1995) was used to estimate the mean of the log hydraulic conductivity distribution (or more conveniently the geometric mean μ_g of the hydraulic conductivity distribution) in such a way that the effective horizontal hydraulic conductivity of the heterogeneous fields will correspond to the homogeneous (and isotropic) value obtained by the calibration of the deterministic model ($K_{eff}^x = 5 \times 10^{-5} m/s$) in the previous section (The numerical model). It is worth noting that the calibration of the hydraulic conductivity field was based on pumping test data (which can also be used directly to calculate the mean hydraulic conductivity). So, the effective directional hydraulic conductivity tensor of the heterogeneous fields can be estimated with Ababou (1995) formula:

$$K_{eff}^i = \mu_g \exp\left(\sigma_{\ln k}^2 \left[\frac{1}{2} - \frac{1}{N} \frac{\lambda_h}{\lambda_i}\right]\right) \quad (1)$$

where μ_g is the geometric mean of the hydraulic conductivity in m/s; $\sigma_{\ln k}^2$ is the $\ln(K)$ variance; N is the number of dimensions; λ_i is the correlation length (in m) in the direction i , and λ_h is the harmonic mean of the correlation lengths (m). Then the mean of the log hydraulic conductivity distribution μ_g can be expressed by:

$$\mu_g = K_{eff}^x \exp\left(\sigma_{\ln k}^2 \left[-\frac{1}{2} + \frac{\lambda_y \lambda_z}{\lambda_y \lambda_z + \lambda_x \lambda_z + \lambda_x \lambda_y}\right]\right) \quad (2)$$

where λ_x , λ_y , and λ_z are the correlation lengths in the principal directions of anisotropy.

Knowing the parameters of the distribution, it was possible to randomly generated as many values of $\ln(K)$ as the number of 1 m interval of the boreholes lengths described

on the geological logs. Then, those random samples were sorted (Fig. 6c). The smaller values were attributed randomly to the less permeable lithofacies (the clay-dominant), the intermediate values were attributed to the sandstone, and the most permeable values were attributed to the sand dominant. It is worth noting that the range of hydraulic conductivity values which will be attributed to the lithofacies was also compared to the corresponding values obtained from the slug test in those lithofacies when this was possible (very often the wells cross multiple lithofacies). This allowed simulating the vertical variations of hydraulic conductivity for each geological log (Fig. 6b) in agreement with the measured data.

In addition, the Pliocene formation in the Korba plain is known to be slightly dipping toward the sea ($1-5^\circ$) and made of elongated layers parallel to the sea as described for example in Allen and Allen (1990). It is expected that the length of these bars is between 2 and 12 km, that they have a width between 2 and 4 km, and a thickness of a few meters. The computation of experimental variograms on the hydraulic conductivities generated as described in the preceding confirmed that these orders of magnitude were reasonable as they showed horizontal correlation lengths in the order of 2–4 km and a few meters in the vertical direction. Furthermore, the data showed a geometric anisotropy in the horizontal plane with a correlation length parallel to the coast about 2 times larger than in the direction perpendicular to the coast. Because the variograms are not based directly on actual measurements, the correlation lengths cannot be estimated accurately. This parameter uncertainty was therefore taken into account by considering several possible combinations of the correlation lengths in the different directions (Table 2; and Fig. 6d).

Assuming a spherical variogram model, the turning-band method (Matheron 1973; Tompson et al. 1989) was used to generate eight simulations for each combination of the possible ranges in the different directions (shown in Table 2). All simulations were conditioned to the 4,423 hydraulic conductivity values simulated along the 36 geological logs. In total, 48 hydraulic conductivity fields were generated (Fig. 7). The simulations were performed using a $200 \times 200 \times 3$ m grid. It is worth noting that the latter resolution is adequate to be directly implemented without scaling operations in the groundwater numerical model which has a similar resolution.

Interaction between uncertainty sources

Before investigating the impact of the uncertainty on the possible long-term evolution of seawater intrusion in the Korba aquifer, the study investigated how the two sources

Table 2 Values of the different sets of correlation lengths used to simulate the hydraulic conductivity fields

Set number	1	2	3	4	5	6
Range perpendicular to the coast [km]	2	2	2	4	4	4
Range parallel to the coast [km]	4	8	12	4	8	12
Vertical range [m]	10	10	10	10	10	10

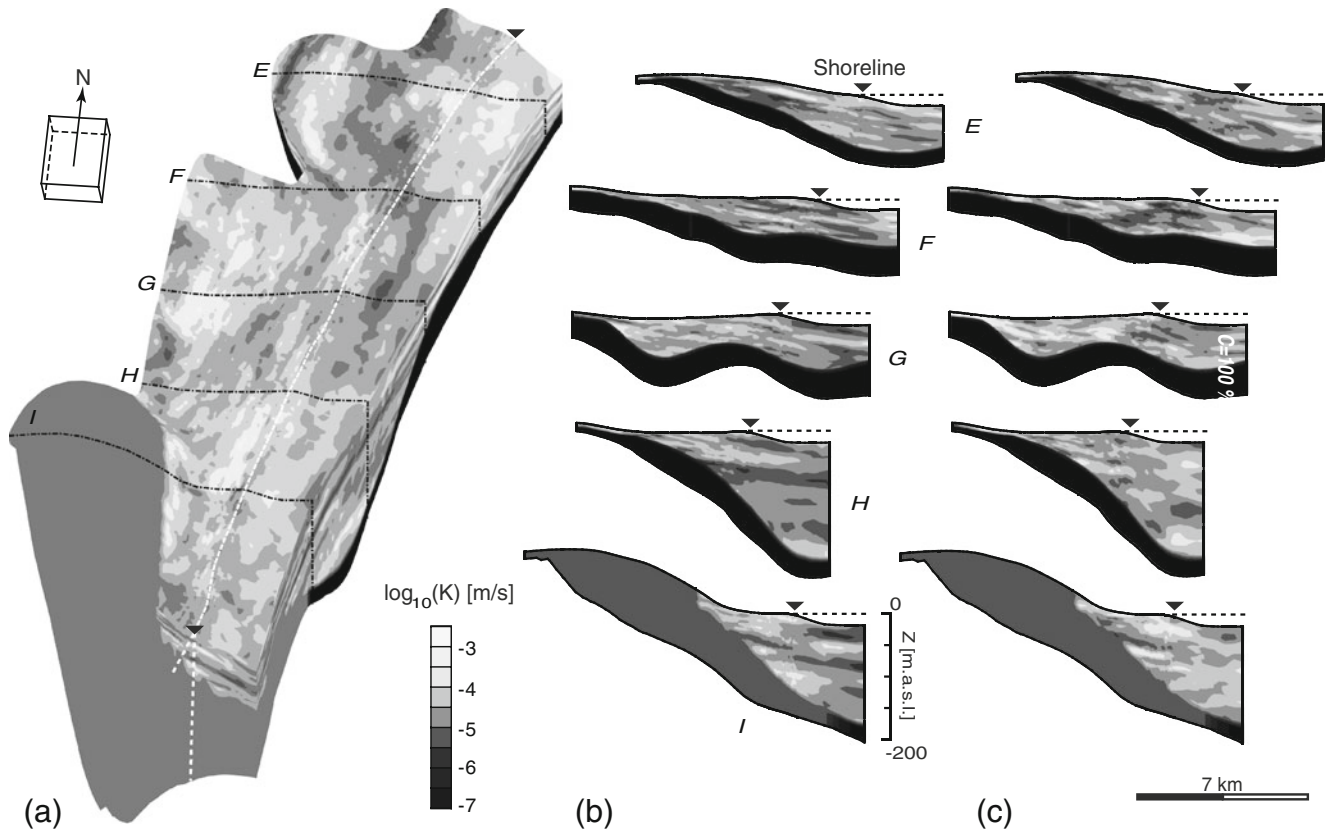


Fig. 7 a 3D view of the decimal logarithm of hydraulic conductivity field with vertical cross sections for two combinations of directional correlation lengths; b $\lambda_x=4$ km, $\lambda_y=12$ km and $\lambda_z=10$ m, and c for $\lambda_x=2$ km, $\lambda_y=4$ km and $\lambda_z=10$ m

of uncertainty interact. This was done by running three sets of Monte Carlo transient simulations for the period 1960–2004. In the first set, only uncertain discharge rate distributions were considered, while in the second set only uncertain hydraulic conductivity fields were considered, and in the last set the joint uncertainties were considered.

For the first set, the hydraulic conductivity field was kept equal to the one obtained by calibration (Table 1). For the second set, the extraction rate field was the simulated distribution that gave a response which was the closest to the ensemble average (in terms of concentrations and heads) in the first set of simulations. For the third set, all the combinations between six simulations of pumping rates and six simulations of the hydraulic conductivity fields were used. The third set allowed analyzing the joint effects of uncertain pumping rates and uncertain hydraulic conductivity on model outputs. The six fields of pumping rate and of hydraulic conductivity were sampled in such a way that they correspond to regular probability intervals covering the cumulative density functions of the maximum drawdown computed for the first and second set of Monte Carlo simulations.

For all the simulations, the initial head and salt distributions had been previously computed in steady state so that they were physically consistent with the hydraulic conductivity field used in the corresponding realization. All other flow and transport parameters as well as time-dependent boundary conditions remained

unchanged. For each simulation, the *GroundWater* finite element code (Cornaton 2007) was used to solve the density-dependent flow and mass-transport problem. Each single simulation required more than 55 h of computing time on a Linux AMD Opteron 64-bit machine. To circumvent the large computing time required to achieve the uncertainty analysis, Monte Carlo simulations were executed concurrently on a 64-processor Linux cluster. The resulting outputs were then post-processed to obtain ensemble statistics.

Globally, all the simulations for the three sets and their respective ensemble averages display the main features observed in the measurements collected in 2004: the central depression, higher levels on the southern and northern part of the aquifer, and a penetration of the seawater wedge of about 2.5 km inland in the central part (Figs. 8 and 9). These similarities, even for increasing correlation scales, result from the use of hydraulic conductivity fields sharing the same effective values, and pumping-rate distributions sharing the same means. A closer look reveals that the head and salt distributions are smoother for the scenarios considering uncertain pumping rates than those considering heterogeneous hydraulic conductivity (Fig. 8). This reflects the spatial variability of the flow velocities due to the heterogeneity. As expected, the ensemble average maps of heads and concentrations (Fig. 9) are different from the maps computed using the average pumping rates and the

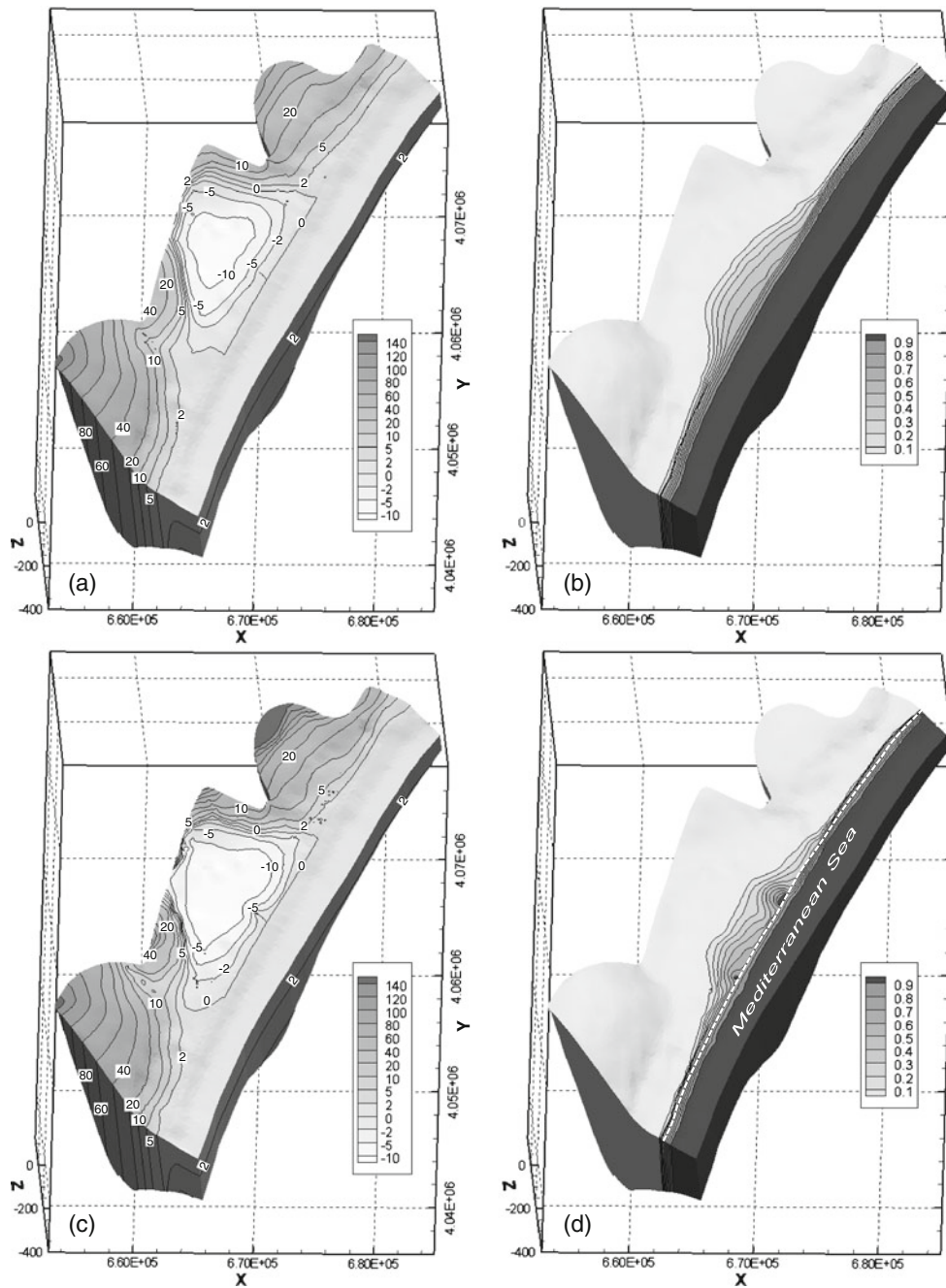


Fig. 8 Examples of **a** and **c** simulated heads (m) and **b** and **d** relative concentrations [-] for variable pumping rate (**a** and **b**) and heterogeneous hydraulic conductivity field (**c** and **d**)

homogeneous permeability field, which is due to the nonlinearity of the flow and transport equations. However, as shown for example by Delhomme (1979), the ensemble averages are the correct estimations of the mean head and concentration distributions, while the solutions resulting from using average inputs are biased. The convergence of ensemble statistics of the heads and concentrations was checked in two randomly chosen wells (Q_{240} and Q_{361}). The maximum drawdown and the influx of seawater over the whole aquifer are the outputs for which the ensemble statistics (mean and variance) of an increasing number of realizations were computed and analyzed. This analysis

showed a faster rate of convergence of the means than the variances, but both reached a satisfactory convergence.

Usually, mean and standard deviation of heads and/or concentrations are used to quantify the uncertainty on model outputs. In this work, it was decided to define criteria which are more tailored to seawater intrusion modelling, where the knowledge of the shape (length and width) of the saltwater wedge is of prime importance. Iso-probability maps corresponding to the probability of a piezometric head below the mean sea level and iso-probability maps corresponding to the probability of a relative concentration greater than 0.1

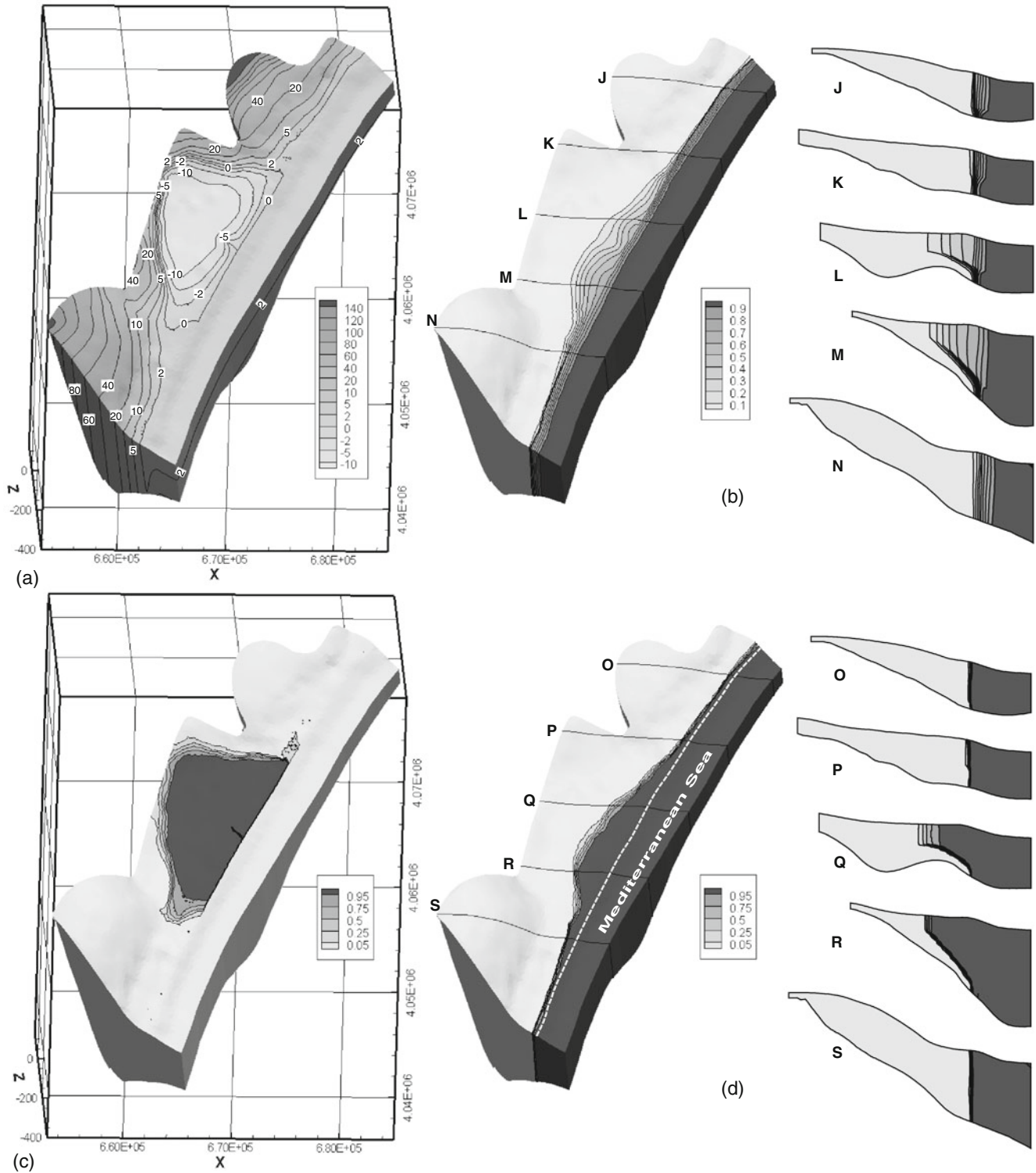


Fig. 9 2004 ensemble averages for the joint uncertainty on pumping rates and hydraulic conductivity: **a** head (m), **b** relative concentration [-]. 2004 probability map for a point **c** to be below the mean sea level and **d** to exceed the 0.1 relative salt concentration

were computed (Fig. 9) for the three sets of simulations. The uncertain areas correspond to intermediate probabilities. Thus, two global dimensionless indicators were computed: U_H [-] and U_C [-]. U_H represents the ratio of the area (km^2) delineated by the 0.05 and 0.95 iso-probability of being below sea

level ($\text{Area}(0.05 \leq P(H < 0) \leq 0.95)$) normalized by the onshore area of the aquifer ($A=328 \text{ km}^2$). This can be expressed by:

$$U_H^i[-]=\text{Area}(0.05 \leq P(H < 0) \leq 0.95)/A \quad (3)$$

with $i \in \{K, Q, KQ\}$ where Q is used when the pumping rates are considered as uncertain (1st set), K is used when only the hydraulic conductivity field is considered as uncertain (2nd set), and KQ is used when K and Q are considered as uncertain.

Similarly U_C represents the percentage of the extension of the aquifer where the probability of exceeding a relative concentration of 0.1 is between 0.05 and 0.95.

$$U_C^i[-] = \text{Area}(0.05 \leq P(C > 0.1) \leq 0.95) / A \quad (4)$$

The results of this analysis are the following:

- In all cases the uncertainties in 2004 are lower than 10 % (Fig. 10), which is less than what was expected.
- The uncertainty in heads increases rapidly in response to increasing pumping rates while the uncertainty in concentrations has a steady growth (Fig. 10), which is explained by the faster response of the flow equation as compared to the transport equation. In addition, the magnitudes of the two uncertainties are different because of the different extensions of the domain affected by the process: the seawater intrusion occurs only on a strip along the coast, while the piezometry reacts almost everywhere in the domain (and not along the coast).
- The uncertainty in concentration is controlled mainly by the uncertainty in the hydraulic conductivity field ($U_C^{QK} \approx U_C^K$, Fig. 10).
- The uncertainties on heads, due either to the uncertainty in extraction rates or heterogeneity, are of the same order of magnitude ($U_H^Q \approx U_H^K$, Fig. 10) but the joint effect is smaller than the sum of the two effects ($U_H^{QK} < U_H^K + U_H^Q$, Fig. 10).
- Because the system is highly non-linear, and with transient boundary conditions, the different sources of uncertainty can become dominant at different time

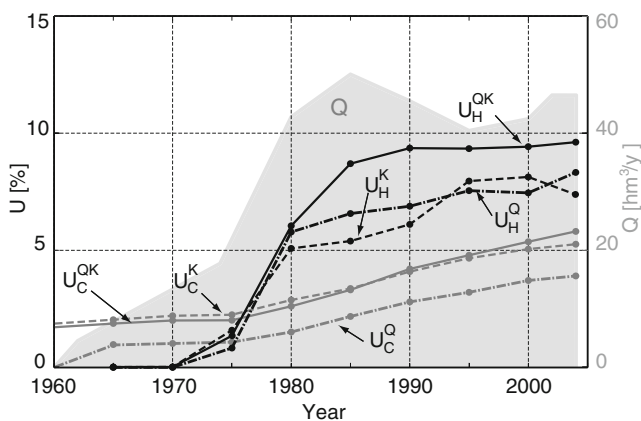


Fig. 10 Progression of the uncertainties during the simulated period: Q (gray background) are the total estimated exploitation volumes (hm^3/y), U_H^{QK} and U_C^{QK} (solid black and gray lines, respectively) represent the scenario of combined uncertainties, U_H^K and U_C^K (dashed black and gray lines, respectively) represent the scenario of uncertain hydraulic conductivity field and U_H^Q and U_C^Q (dash-point black and gray lines, respectively) represent the scenario of uncertain pumping rates

steps. For example, $U_H^Q > U_H^K$ in 1985 and $U_H^Q < U_H^K$ in 2000 (Fig. 10). Therefore, one cannot assume that one source of uncertainty will always be the main one.

Additional comparisons of the local probability density functions obtained under the three sets of Monte Carlo simulations indicate that there is no simple way to decouple and simplify the analysis of the uncertainty. This will lead us, in the next section, to consider only the case of joint uncertainty.

Forecasts of seawater intrusion from 2004 to 2048

Definition of the scenarios

According to the Tunisian Institute of Statistics (INS 2007), the Tunisian population will grow from 9.93 million inhabitants in 2004 to 12.74 million in 2034. This demographic growth will increase freshwater stress, especially on groundwater, over the whole country.

At the same time, most of the global climate change models (Bates et al. 2008) predict decreasing precipitation and increasing temperatures and hence evapotranspiration in the Mediterranean region for the next century, which will affect the hydrological cycle in many countries. In Tunisia, a reduction of 20–25 % of the annual average precipitation is expected for 2050 (Ragab and Prudhomme 2002), which means that the precipitation in the study area will decrease from 420 mm/y to 315–336 mm/y. Since the hydrological cycle is highly non-linear, 20 % of reduction of the annual rain does not necessarily mean that the recharge of the aquifer will be reduced by 20 %. The methodology used for the estimation of the recharge, described in the previous (i.e. Thornthwaite and Mather method with daily time step and with accounting for distributed soil properties), was used to investigate the effects of constant (in time) reduction of the annual rain. The results showed that 5, 10 and 20 % of reduction of the annual rain result in 20, 36 and 61 % of reduction of the aquifer recharge, respectively. Given all the uncertainty affecting the recharge estimation as well as its long-term forecasts, the natural recharge of the aquifer was assumed to be reduced by at least 20 % in 2050 both for the direct infiltration and for the recharge from the underlying aquifers.

In addition to the increasing freshwater demand and a possible reduction of the recharge of the aquifer expected for 2050, the Mediterranean Sea will most probably rise at a rate of about 2.5 mm/y on average for the next century (Mangiarotti 2003; Ranjan et al. 2006; Bates et al. 2008). However, exploratory simulation showed that this phenomenon is expected to have a limited impact in Cape Bon during the time frame of the scenario (11 cm sea-level rise in 2048).

In order to forecast the response of the Korba aquifer to a reduction of the natural recharge and to different management scenarios, long-term stochastic forecasts were carried out. Two scenarios were considered:

- Scenario 1: the recharge is reduced linearly and progressively so that the recharge in 2048 will be 24 hm³/y, which represents 20 % less than the recharge in 2004. The pumping rates of 2004 (47 hm³/y) are kept constant until 2048. This would be a continuation of the 2004 state of exploitation. Note that the pumping rates remained constant since the late 1980s (Fig. 10). Because this rate of exploitation corresponds to the continuation of a clear over-exploitation of the system—the total extraction estimated in 2004 corresponds to about 135 % of the recharge—this scenario is considered as the worst-case scenario.
- Scenario 2: the recharge is reduced linearly as for scenario 1 but the pumping rates as well are reduced linearly to reach the amount of recharge expected in 2048, which represents a progressive reduction of the pumping rates by 50 %.

The sea level rise was considered less dangerous than the other threats and was not accounted for. Considering these two scenarios, Monte Carlo simulations were continued from 2004 to 2048 with the scenario of uncertain pumping rates and uncertain hydraulic conductivity field. For reasons of consistency with reality, a concentration threshold was attributed to constrain pumping wells: pumps are deactivated ($Q=0$) if the concentration of pumped water exceeds a relative concentration of 0.2 ($C>0.2$), and restarted for a concentration less than 0.1 (this threshold was taken because it corresponds to the limit below which some plants still tolerate such high concentrations of 6–7 kg/m³ and farmers can still use it for irrigation by mixing it with less saline water to save freshwater reserves).

Results

Figures 11 and 12 show the ensemble averages of hydraulic heads and relative salt concentrations as well as the probability maps for the first and second scenarios. Those statistics were calculated from 36 Monte Carlo simulations for each scenario.

In addition to the uncertainty norms U_H and U_C defined in the previous, and in order to evaluate the consequences of each scenario, the area of the aquifer where the relative salt concentrations exceed 0.1 was calculated and normalized by the onshore surface of the aquifer, which gives $S^{C>0.1}$. Similarly, the normalized area of the aquifer where heads are below sea level was calculated too, which gives $S^{H<0}$. These dimensionless indicators were computed for all the simulations in order to obtain their statistical distributions. The results are summarized in Table 3.

If one compares first the forecasts in 2048 for both scenarios with the state of the aquifer estimated in 2004, one finds that in all cases the surface affected by seawater intrusion will increase significantly, until reaching between 30 and 41 % of the aquifer, while it was estimated to cover between 21 to 26.5 % of the aquifer in 2004 (Table 3). The estimated uncertainty will also rise in both cases. It is worth noting that due to the constraint of

concentrations in wells ($Q=0$ if $C>0.2$), a large number of wells were turned off and the total pumping in 2048 was reduced by 7 %.

When comparing the forecasts made for the two scenarios, the results show that progressively reducing the pumping rates over the whole aquifer by 50 % until 2048 will affect the heads distribution more than the salt concentrations distribution. The area $S^{H<0}$, where heads are below sea level, will be reduced significantly from 29.7 to 11.6 % (at a probability level of 0.5), while the area $S^{C>0.1}$ will be reduced only from 37.5 to 33.7 % (same probability level). This is expected for two reasons. First, as long as the hydraulic gradients will still be oriented landward (Fig. 12a), the seawater wedge will continue to penetrate further inland even if the piezometric depression is smaller. Furthermore, dispersion is not a reversible phenomenon. Consequently, the time scale required to naturally clean up a coastal aquifer that was invaded by seawater intrusion is usually much longer than the time scale required for the invasion. This was shown in the work by Kerrou et al. (2010a) where the time required for the 0.25 iso-concentration to recede back to its natural state was estimated to be more than 1.5 centuries after the complete stop of 45 years of pumping. The reduction of the pumping rates by half until 2048 will therefore reduce the saltwater intrusion velocity but will not stop it. Most probably ($P=0.95$), an additional 30 km² (9.5 % of the surface of the aquifer) will be affected by higher concentrations ($C>0.1$) as compared to the situation in 2004. Those computations show that the time-lag involved in seawater intrusion and recession is very important and has to be considered for planning groundwater and land use.

Summary and conclusions

This study investigated how the uncertainties on the spatial distribution of pumping rates and hydraulic conductivities can affect the knowledge of the current state and evolution of a coastal aquifer. The methodology included a stochastic model for the pumping rates and one for the hydraulic conductivity. For the setup of the geostatistical model of hydraulic conductivities, a multi-Gaussian distribution with geometric anisotropy was assumed. The stochastic model of the pumping rates was based on a multivariate linear regression and a geostatistical model of the residuals. The propagation of these uncertainties to predictions of heads and concentrations in the aquifer was carried out by Monte Carlo simulations using a 3D numerical model of density-dependent flow and mass transport. This was made possible by using a high performance Linux cluster in this work and grid computing in a preliminary study (Kerrou et al. 2010b). The two sources of uncertainty were evaluated separately and jointly in order to investigate how they interact. The stochastic model was then used to forecast the head and salt concentration distributions in 2048 for two management scenarios.

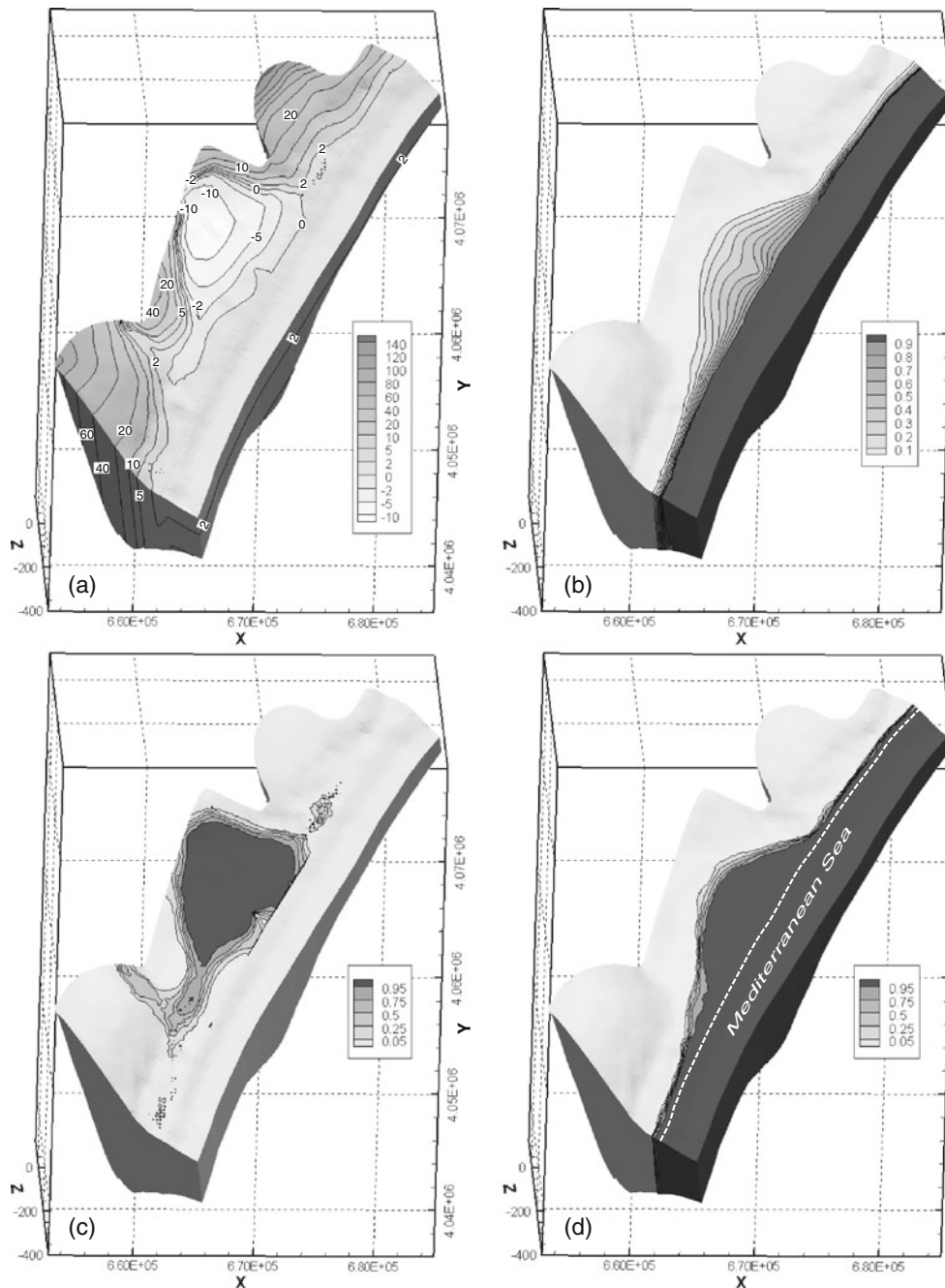


Fig. 11 2048 scenario 1 forecasts: Ensemble averages: **a** head (m) **b** relative concentration [-] maps for the 36 realizations; Probability maps for a point **c** to be below the mean sea level and **d** to exceed the 0.1 relative salt concentration

It was found that the uncertainty in the hydraulic conductivity distribution had more impact on the transport predictions than the uncertainty in the spatial distribution of the discharge rates. Both sources of uncertainty affected similarly the flow predictions but slight differences could be seen when looking at the time evolution of those uncertainties. Similarly, the uncertainties on flow and transport predictions behave differently as a function of time. The uncertainty in heads react generally faster and show stronger responses than those on concentrations when the pumping rates evolve. The combined effects of the two sources of uncertainty had more

impact on the flow predictions than on the transport predictions.

From a practical point of view, the results showed that if the pumping rates remain at their 2004 level in the Korba aquifer and if recharge is reduced by 20 % due to climate change, then there is a high probability ($P=0.95$) that at least 12.8 % of the surface of the aquifer will be additionally contaminated in 2048. Reducing the pumping rates progressively by 50 % until 2048 will not result in a recession of the saltwater wedge; instead an additional 9.5 % (30 km²) of the surface of the aquifer will be contaminated in 2048 especially in the central part of the

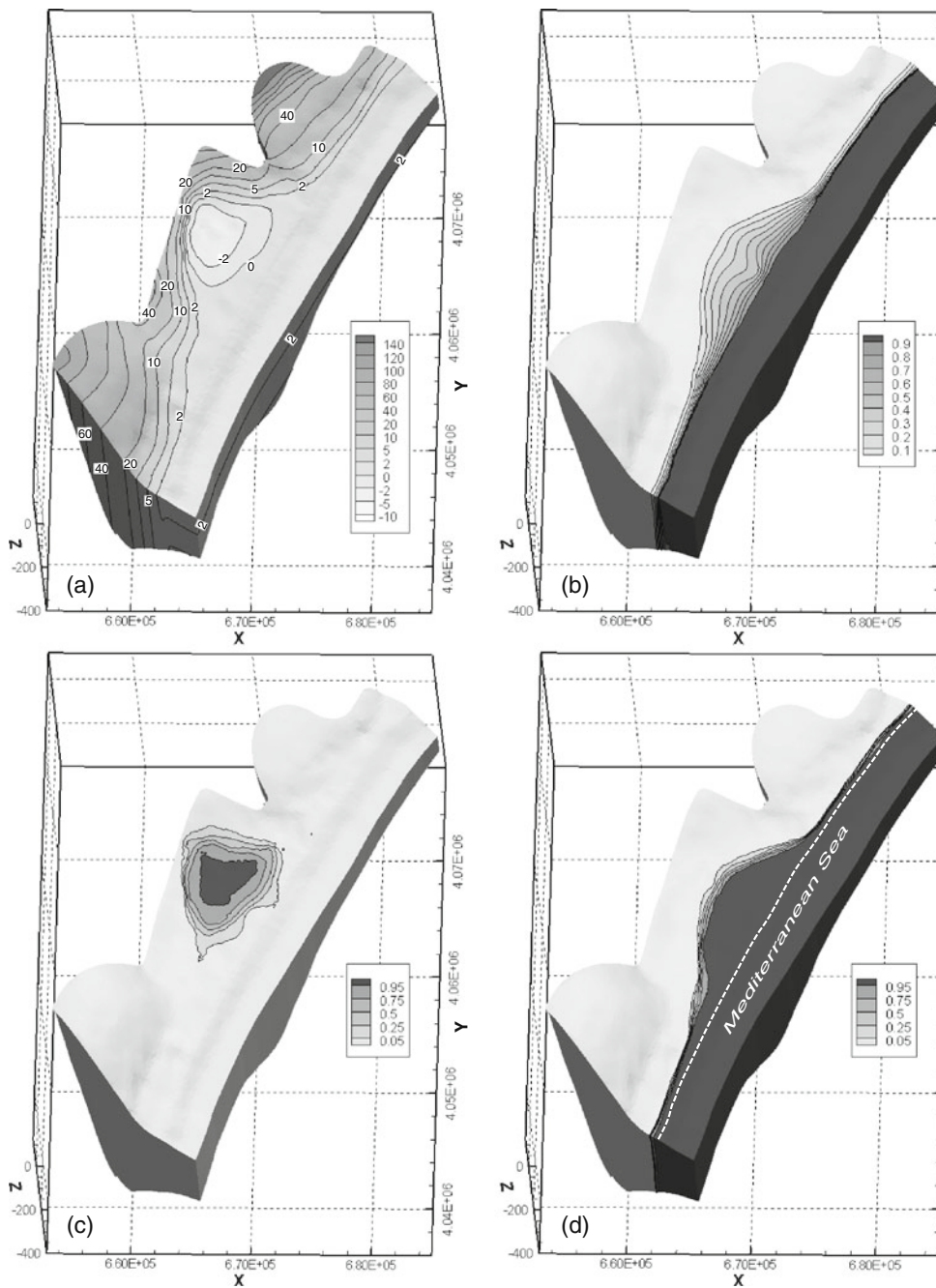


Fig. 12 2048 scenario 2 forecasts: Ensemble averages **a** head (m) **b** relative concentration [-] maps for the 36 realizations; Probability maps for a point **c** to be below the mean sea level and **d** to exceed the 0.1 relative salt concentration

Table 3 Summary of the stochastic modelling and forecasts results

		State in 2004			Forecast in 2048	
		Uncert. Q	Uncert. K	Joint Uncert.	Scenario 1	Scenario 2
$S^{H<0}$ [%]	$P=0.95$	27.8	29.8	28.0	21.9	4.1
	$P=0.5$	32.0	33.2	32.8	29.7	11.6
	$P=0.05$	36.1	37.4	37.7	40.7	18.8
$S^{C>0.1}$ [%]	$P=0.95$	23.8	21.2	20.7	33.5	30.2
	$P=0.5$	25.8	23.7	23.4	37.5	33.7
	$P=0.05$	27.7	26.5	26.5	41.3	37.1
U_C [%]		3.9	5.3	5.8	7.8	6.9
U_H [%]		8.3	7.6	9.6	18.8	14.6

aquifer. The Korba area is therefore potentially subject to important future losses in the agricultural sector. Furthermore, the situation will continue to deteriorate after 2048 in this scenario.

One way to avoid the progressive deterioration of the groundwater quality that will affect the aquifer for tens of years and to reach a possible sustainable situation would be to re-allocate the groundwater extraction to ensure the complete recovery of the central depression. Indeed, the northern and southern parts of the aquifer are still showing high piezometric levels and could be exploited more. The different projects related to artificial recharge (from surface water and treated wastewater) currently implemented in the region have a positive impact at a local scale but are an order of magnitude too small to have a significant influence on the central depression. This is why a feasible approach would be to increase the extraction in the north and the south and to reduce it in the centre. Water transfer from northern regions and usage of surface water from the dams could be used to compensate the problems due to reduced extraction in the central part. The maximum amounts that could be exploited in each part of the aquifer could, therefore, be estimated by optimization based on the model described in this study in conjunction with cost analysis. This could provide the base for supporting long-term policy analysis and strategic decision making for integrated and sustainable development in the Korba region.

Acknowledgments This work has been funded by the Swiss National Science Foundation under Grants: 207020-110017 and PP002-106557. The authors thank Ghislain de Marsily, Rachid Ababou, Jesus Carrera as well as Ellen Milnes and Philip Brunner for providing valuable suggestions on the manuscript. The authors are also grateful to Gregoire Mariethoz and three anonymous reviewers for their constructive comments.

References

- Ababou R (1995) Random porous media flow on large 3-D grids: numerics, performance and application to homogenization. In: Wheeler MF (ed) *Environmental studies: mathematical, computational and statistical analysis*. IMA Volumes in Mathematics and its Applications, Springer, New York, pp 1–25
- Abarca E (2006) *Seawater intrusion in complex geological environments*. PhD Thesis, Technical University of Catalonia, Spain
- Abarca E, Vazquez-Sune E, Carrera J, Capino B, Gamez D, Batlle F (2006) Optimal design of measures to correct seawater intrusion. *Water Resour Res* 42:W09415. doi:10.1029/2005WR004524
- Abarca E, Carrera J, Sánchez-Vila X, Dentz M (2007) Anisotropic dispersive Henry problem. *Adv Water Resour* 30:913–926. doi:10.1016/j.advwatres.2006.08.005
- Al-Bitar A, Ababou R (2005) Random field approach to seawater intrusion in heterogeneous coastal aquifers: unconditional simulations and statistical analysis. In: Renard P, Demougeot-Renard H, Froidevaux R (eds) *Geostatistics for environmental applications*. Springer, Heidelberg, Germany
- Alcolea A, Renard P, Mariethoz G, Bertone F (2009) Reducing the impact of a desalination plant using stochastic modeling and optimization techniques. *J Hydrol* 365(3–4):275–288
- Allen PA, Allen JR (1990) *Basin analysis: principles and applications*. Blackwell, Oxford
- Arfib B, de Marsily G, Ganoulis J (2002) Coastal karst springs in the Mediterranean basin: study of the mechanisms of saline pollution at the Almyros spring (Crete), observations and modelling. *Bull Soc Geol Fr* 173(3):245–253
- Bates BC, Kundzewicz ZW, Wu S, Palutikof JP (2008) *Climate change and water*. Technical paper of the Intergovernmental Panel on Climate Change. IPCC Secretariat, Geneva, 210 pp
- Bear J, Cheng AHD, Sorek S, Ouazar D, Herrera I (1999) *Seawater intrusion in coastal aquifers: concepts, methods and practices*. Kluwer, Dordrecht, The Netherlands
- Ben Hamouda M, Tarhouni J, Leduc C, Zouari K (2011) Understanding the origin of salinization of the Plio-quaternary eastern coastal aquifer of Cap Bon (Tunisia) using geochemical and isotope investigations. *Environ Earth Sci* 63(5):889–901
- Brunner P, Kinzelbach W (2008) *Sustainable Groundwater Management*. *Encycl Hydrol Sci*. doi:10.1002/0470848944.hsa164
- Cheng AHD, Halhal D, Naji A, Ouazar D (2000) Pumping optimization in saltwater-intruded coastal aquifers. *Water Resour Res* 36(8):2155–2165
- Cooper HH, Bredehoeft JD, Papadopulos SS (1967) Response of a finite-diameter well to an instantaneous charge of water. *Water Resour Res* 3(1):263–269
- Cornaton F (2007) *GroundWater: a 3-D ground water flow and transport finite element simulator*. Reference manual, 190pp. <http://www1.unine.ch/chyn/php/software.php>. Accessed August 2008
- Custodio E (2002) Aquifer overexploitation: what does it mean? *Hydrogeol J* 10(2):254–277
- Dagan G, Zeitoun DG (1998) Seawater–freshwater interface in a stratified aquifer of random permeability distribution. *J Contam Hydrol* 29(3):185–203
- Delhomme JP (1979) Spatial variability and uncertainty in groundwater-flow parameters: geostatistical approach. *Water Resour Res* 15(2):269–280
- DGRE (2000) *Rapport d'exploitation des nappes phréatiques de l'année 2000*. Direction Générale des Ressources en Eau [Report on the exploitation of groundwater in 2000. General Directorate of Water Resources]. Ministère de l'agriculture et des ressources hydrauliques, Tunis, Tunisia
- Diersch H-JG, Kolditz O (2002) Variable-density flow and transport in porous media: approaches and challenges. *Adv Water Resour* 25(8–12):899–944
- Doherty J (1998) *PEST-Model independent parameter estimation*. Watermark Numerical Computing, Brisbane, Australia
- Eckhardt K, Ulbrich U (2003) Potential impacts of climate change on groundwater recharge and streamflow in a central European low mountain range. *J Hydrol* 284(1–4):244–252
- Elder JW (1958) Numerical experiments with a free convection in a vertical slot. *J Fluid Mech* 24:823–843
- Ennabli M (1980) *Etude hydrogéologique des aquifères du nord-est de la Tunisie pour une gestion intégrée des ressources en eau* [Hydrogeological study of aquifers of northeast Tunisia for the integrated management of water resources]. PhD Thesis, Université de Nice, France
- Essink G (2001) Salt water intrusion in a three-dimensional groundwater system in the Netherlands: a numerical study. *Transp Porous Media* 43(1):137–158
- Grava M (2005) *Hydrochemical, hydrogeological, and geostatistical analysis of Eastern Cape Bon aquifer (northern Tunisia)*. Postgraduate Thesis, Centre d'hydrogéologie de l'Université de Neuchâtel, Switzerland
- Hassan A, Pohlmann K, Chapman J (2001) Uncertainty analysis of radionuclide transport in a fractured coastal aquifer with geothermal effects. *Transp Porous Media* 43(1):107–136
- Held R, Attinger S, Kinzelbach W (2005) Homogenization and effective parameters for the Henry problem in heterogeneous formations. *Water Resour Res* 41:1–14. doi:10.1029/2004WR003674
- Hendricks Franssen HJ (2009) The impact of climate change on groundwater resources. *Int J Cli Chang Strateg Manag* 1(3):241–254

- Henry HR (1964) Effects of dispersion on salt enrichment in coastal aquifers. In: Sea water in coastal aquifers. US Geol Surv Water Supp Pap 1613-C, pp 70–84
- Holman IP (2006) Climate change impacts on groundwater recharge-uncertainty, shortcomings, and the way forward? *Hydrogeol J* 14(5):637–647
- Hvorslev MJ (1951) Time lag and soil permeability in ground-water observations, Bull. No. 36, Waterways Exper. Sta., US Army Corps of Eng., Vicksburg, MS, pp 1–50
- INS (2007) Prévisions sur l'évolution de la Population 2004-2034 [Predictions about the evolution of the population 2004-2034]. Institut National de la Statistique, Tunis, Tunisia. <http://www.ins.nat.tn/>. Accessed August 2012
- Iribar V, Carrera J, Custodio E, Medina A (1997) Inverse modelling of seawater intrusion in the Llobregat delta deep aquifer. *J Hydrol* 198(1–4):226–244
- Kerrou J, Renard P (2010) A numerical analysis of dimensionality and heterogeneity effects on advective dispersive seawater intrusion processes. *Hydrogeol J* 18(1):55–72. doi:10.1007/s10040-009-0533-0
- Kerrou J, Renard P, Tarhouni J (2010a) Status of the Korba groundwater resources (Tunisia): observations and 3D modelling of seawater intrusion. *Hydrogeol J* 18(5):1173–1190. doi:10.1007/s10040-010-0573-5
- Kerrou J, Renard P, Lecca G, Tarhouni J (2010b) Grid-enabled Monte Carlo analysis of the impacts of uncertain discharge rates distribution on seawater intrusion in the Korba aquifer (Tunisia). *Hydrol Sci J* 55(8):1325–1336. doi:10.1080/02626667.2010.519706
- Khlaifi I (1998) Contribution à l'étude de l'intrusion marine par un modèle de transport tridimensionnel: interfaçage avec des systèmes d'information géographique [Contribution to the study of seawater intrusion using a three-dimensional transport model interfacing with GIS]. MSc Thesis, Institut National Agronomique de Tunisie, Tunisia
- Kouzana L, Ben Mammou A, Sfar Felfoul M (2009) Seawater intrusion and associated processes: case of the Korba aquifer (Cap-Bon, Tunisia). *C R Geosci* 341(1):21–35
- Lecca G, Petitdidier M, Hluchy L, Ivanovic M, Kussul N, Ray N, Thieron V (2011) Grid computing technology for hydrological applications. *J Hydrol* 403(1–2):186–199
- Mangiarotti S (2003) Les variations basse fréquence du niveau de la mer Méditerranée au cours de la deuxième moitié du XXe siècle par altimétrie spatiale et marégraphie [Low-frequency variations in the Mediterranean Sea level during the second half of the twentieth century by satellite altimetry and tide gauge]. PhD Thesis, Université de Toulouse III – Paul Sabatier, France
- Mantoglou A, Papantoniou M, Giannouloupoulos P (2004) Management of coastal aquifers based on nonlinear optimization and evolutionary algorithms. *J Hydrol* 297(1–4):209–228
- Mariethoz G, Renard P, Comaton F, Jaquet O (2009) Truncated plurigaussian simulations to characterize aquifer heterogeneity. *Ground Water* 47(1):13–24. doi:10.1111/j.1745-6584.2008.00489.x
- Matheron G (1973) The intrinsic random functions and their applications. *Adv Appl Probab* 5(3):439–468
- Milnes E (2011) Process-based groundwater salinisation risk assessment methodology: application to the Akrotiri aquifer (southern Cyprus). *J Hydrol* 399(1–2):29–47
- Naji A, Cheng AHD, Ouazar D (1998) Analytical stochastic solutions of saltwater/freshwater interface in coastal aquifers. *Stoch Hydrol Hydraul* 12(6):413–430
- Oueslati A (1994) Les côtes de la Tunisie. Recherche sur leur évolution au Quaternaire [The coast of Tunisia. Research on its evolution during the Quaternary]. Imprimerie officielle de la République Tunisienne, Tunis
- Paniconi C, Khlaifi I, Lecca G, Giacomelli A, Tarhouni J (2001) Modeling and analysis of seawater intrusion in the coastal aquifer of eastern Cap-Bon, Tunisia. *Transp Porous Media* 43:3–28
- Pohlmann KF, Hassan AE, Chapman JB (2002) Modeling density-driven flow and radionuclide transport at an underground nuclear test: uncertainty analysis and effect of parameter correlation. *Water Resour Res* 38(5)
- Ragab R, Prudhomme C (2002) Climate change and water resources management in arid and semi-arid regions: prospective and challenges for the 21st century. *Biosyst Eng* 81(1):3–34
- Ranjan P, Kazama S, Sawamoto M (2006) Effects of climate change on coastal fresh groundwater resources. *Glob Environ Chang* 16(4):388–399
- Reilly TE, Goodman AS (1985) Quantitative-analysis of saltwater fresh-water relationships in groundwater systems: a historical-perspective. *J Hydrol* 80:125–160
- Renard P (2007) Stochastic hydrogeology: what professionals really need? *Ground Water* 45(5):531–541. doi:10.1111/j.1745-6584.2007.00340.x
- Scibek J, Allen DM (2006) Modeled impacts of predicted climate change on recharge and groundwater levels. *Water Resour Res* 42, W11405
- Sherif MM, Singh VP (1999) Effect of climate change on sea water intrusion in coastal aquifers. *Hydrol Processes* 13(8):1277–1287
- Slama F, Milnes E, Bouhlila R (2008) Calibrating unsaturated model parameters using electrical resistivity tomography imaging. In: Refsgaard JC, KK, Haarder E, Nygaard E (eds) Calibration and reliability in groundwater modelling: Credibility of modelling. IAHS Publ. 320, IAHS, Wallingford, UK, pp 148–153
- Steenhuis TS, Van der Molen WH (1986) The Thornthwaite-Mather procedure as a simple engineering method to predict recharge. *J Hydrol* 84:221–229
- Tarhouni J, Jemai S, Walraevens K, Rekaya M (1996) Caractérisation de l'aquifère côtier de Korba au Cap Bon (Tunisie) [Characterisation of the coastal aquifer of Korba Cape Bon (Tunisia)]. Progress report 95-96 for AVI-73 EC Project, Ghent University, Ghent, Belgium
- Tompson AFB, Ababou R, Gelhar LW (1989) Implementation of the 3-dimensional turning bands random field generator. *Water Resour Res* 25:2227–2243
- Werner A (2010) A review of seawater intrusion and its management in Australia. *Hydrogeol J* 18(1):281–285
- Werner A, Simmons G (2009) Impact of sea-level rise on sea water intrusion in coastal aquifers. *Ground Water* 47(2):197–204